COMPUTER METHODS IN APPLIED MECHANICS AND ENGINEERING 77 (1989) 293–310
NORTH-HOLLAND

ANALYSIS OF CONCRETE STRUCTURES UNDER THERMAL LOADING

René de BORST and Paul P.J.M. PEETERS
Delft University of Technology, Department of Civil Engineering /
TNO Institute for Building Materials and Structures, Delft, The Netherlands

Received 23 December 1988
Revised manuscript received 29 May 1989

The material behaviour of concrete at elevated temperatures is highly nonlinear since thermal dilatation, temperature-dependent material properties, transient creep and cracking all play an important role. For reinforced and prestressed concrete structures there is the added complication that the material properties of the reinforcing steel are also a strongly nonlinear function of the temperature. In this contribution an algorithm is developed which treats these phenomena in a unified concept. It includes a generalised mid-point rule as a time integrator, the accuracy of which has been assessed for forward, fully backward and mid-point integration strategies. Proper linearisation moduli have been set up which ensure that the algorithm converges quadratically on a structural level if Newton's method is used. The model has been tested against some tests on plain concrete specimens and has been compared with an experiment on a one-way reinforced concrete slab.

1. Introduction

The behaviour of concrete structures that are exposed to thermal loading is an issue of great practical importance. Indeed, a considerable amount of literature exists with regard to the behaviour of plain concrete as well as reinforcement at elevated temperatures [1–9]. Also, a significant number of structural tests are known in which for instance slabs have been brought to failure by exposing them to extreme thermal conditions, e.g. [10]. In consideration of the modern trend to predict the behaviour of structures under extreme circumstances by numerical techniques rather than simulating the behaviour in scale tests it is surprising that numerical simulations are virtually absent in the literature. Only a few contributions have been published which consider numerical simulations of concrete structures under thermal loading, e.g. [11, 12]. This paucity is probably a silent testimony to the difficulties that are involved in properly carrying out such analyses, which obviously must account for cracking, degradation of elastic and inelastic properties with increasing temperature, thermal dilatation, transient creep and yielding of the reinforcement. Most phenomena that are mentioned in the above enumeration may already present considerable numerical difficulties alone. A proper combination of them presents a major challenge to the analyst.

It is the writers' conviction that numerical predictions of large-scale concrete structures such as storage tanks for liquid natural gas are only feasible when a smeared formulation is used for cracking. The classical approach to smeared cracking as pioneered by Rashid [13] and Suidan and Schnobrich [14] then immediately presents difficulties, since it is not well suited for

combination with other nonlinear phenomena, e.g., transient creep, thermal dilatation and degradation of the elastic moduli. Indeed, the use of modern fracture mechanics tools for controlling crack propagation rules out the use of the classical smeared crack approach if constitutive models for phenomena such as mentioned above are employed [15]. This fundamental difficulty can be overcome when the strain decomposition approach [15–19] is followed. In this method the total strain rate is decomposed into a crack and a concrete strain rate. Each strain rate is governed by a separate constitutive law which opens the possibility of constructing a consistent set of rate equations.

To date, little is known about the impact of temperature changes on crack propagation in concrete. Experiments which for instance aim at providing a relation between the fracture energy G_f and the temperature θ are scarce. The few available data suggest a decrease of the fracture energy at elevated temperatures [20], but it is judged to be premature to introduce such a dependence into a constitutive model. For the behaviour of the solid, intact concrete much more is known [1–8], although also in that case there are gaps which should be filled in order to construct a reliable, consistent model. In particular three-dimensional models for transient creep seem to lack a firm experimental basis. In consideration of the importance of the phenomenon of transient creep, i.e., the observation that thermal strains depend not only on the temperature, but also on the applied stress, disregarding this effect in an analysis will severely undermine the capability to accurately predict stresses and strains in concrete structures under transient temperature conditions.

The main purpose of this contribution is to outline a consistent approach to smeared crack analysis of concrete structures which are exposed to extreme thermal conditions. Since it is important that such analyses are based on true material behaviour we will also discuss the constitutive models for the concrete and the reinforcement. Thermal dilatation, degradation of the elastic moduli and strength properties, and transient creep will be discussed. A proper three-dimensional model will be set up for the latter phenomenon and will be calibrated with experimental data. Next, it is discussed how the constitutive relations for the concrete are combined with a smeared crack model in a consistent fashion. The integration to finite time increments is presented and consistent linearisation moduli are derived. Finally, the correlation is made with elementary tests on plain concrete cylinders and with a structural test on a reinforced one-way slab exposed to fire conditions.

2. Transient creep of concrete

During heating of a concrete specimen several nonlinear physical phenomena can be observed. First the material expands. This thermal dilatation is governed by the linear coefficient of thermal expansion α which may be a nonlinear function of the temperature θ. Another important effect is the decrease of the stiffness properties such as Young's modulus E. The latter effect is partly responsible for the observation that a loaded concrete specimen experiences a different change in strains than an initially stress-free specimen. Yet, the change in elastic properties at elevated temperature cannot explain the difference in strain development alone when two concrete specimens, one being stress-free, the other being subjected to an initial stress, are heated. This phenomenon has been investigated thoroughly by Anderberg and Thelandersson [1–3] over the past decade. From their as well as from other investigations

[4–8] it has appeared that during the first heating of a concrete specimen there exists another strain component, which takes place in a very short period of time. This strain component is often named transient thermal strain or transient creep and is a function of the temperature as well as the stress.

It is not yet entirely clear which mechanisms cause the phenomenon of transient creep, but it seems that between 100 and 200°C drying of the cement matrix is the most important factor (drying creep), while for higher temperatures a change of the chemical structure of the cement matrix is primarily responsible for the observed strains (transitional thermal strain). In a one-dimensional context a simple formula has been proposed by Anderberg and Thelandersson [2]. According to this proposal the transient strain $\dot{\boldsymbol{\varepsilon}}^{\mathrm{tr}}$ is given by

$$\dot{\boldsymbol{\varepsilon}}^{\mathrm{tr}} = \frac{\alpha k}{f_{\mathrm{cc}}} \dot{\theta} \boldsymbol{\sigma} , \tag{1}$$

where α is the current value of the linear coefficient of thermal expansion, f_{cc} is the compressive strength at room temperature, $\boldsymbol{\sigma}$ is the uniaxial stress and k is a material parameter, which varies between 1.8 [7, 8] and 2.35 [1–3]. Although hygric influences which are particularly important in the temperature traject between 100 and 200°C are not taken into account explicitly in this model, so that the phenomenon of drying creep is not modelled properly, (1) turns out to be reasonably accurate also for this temperature regime.

For the formulation of a proper three-dimensional model, we shall postulate that the three-dimensional creep rate $\dot{\boldsymbol{\varepsilon}}^{\mathrm{tr}}$ depends linearly on the stress vector $\boldsymbol{\sigma}$. Accordingly, we can write

$$\dot{\boldsymbol{\varepsilon}}^{\mathrm{tr}} = \dot{\theta} \boldsymbol{H} \boldsymbol{\sigma} , \tag{2}$$

with $\boldsymbol{H}$ a constant matrix. If it is assumed that the process of transient creep does not induce any anisotropy, $\boldsymbol{H}$ is given by

$$H_{ijkl} = \frac{\alpha k}{f_{\mathrm{cc}}} \left[-\gamma \delta_{ij} \delta_{kl} + \tfrac{1}{2}(1+\gamma)(\delta_{ik}\delta_{jl} + \delta_{il}\delta_{jk}) \right] , \tag{3}$$

with γ an additional material constant and δ_{ij} the Kronecker symbol.

Thelandersson [3] has also developed a multiaxial generalisation of the model of (1) for transient creep. He has decomposed the transient creep strain rate into a deviatoric part $\dot{\boldsymbol{\varepsilon}}_{\mathrm{d}}^{\mathrm{tr}}$ and a volumetric contribution $\dot{\boldsymbol{\varepsilon}}_{\mathrm{v}}^{\mathrm{tr}}$:

$$\dot{\boldsymbol{\varepsilon}}^{\mathrm{tr}} = \dot{\boldsymbol{\varepsilon}}_{\mathrm{v}}^{\mathrm{tr}} + \dot{\boldsymbol{\varepsilon}}_{\mathrm{d}}^{\mathrm{tr}} , \tag{4}$$

where

$$\dot{\boldsymbol{\varepsilon}}_{\mathrm{v}}^{\mathrm{tr}} = \gamma_{\mathrm{v}} \dot{\theta} p \boldsymbol{i} \tag{5}$$

and

$$\dot{\boldsymbol{\varepsilon}}_{\mathrm{d}}^{\mathrm{tr}} = \gamma_{\mathrm{d}} \dot{\theta} \boldsymbol{s} , \tag{6}$$

p is the hydrostatic pressure (negative for compression), $\boldsymbol{s}$ is the deviatoric stress vector, $\boldsymbol{i} = [1\,1\,1\,0\,0\,0]^{\mathrm{t}}$, and γ_{v} and γ_{d} are material constants. They can be related to the constants k and γ by considering that (4)–(6) can be rewritten to yield

$$\dot{\varepsilon}_{ij}^{\mathrm{tr}} = [\tfrac{1}{3}(\gamma_{\mathrm{v}} - \gamma_{\mathrm{d}})\delta_{ij}\delta_{kl} + \tfrac{1}{2}\gamma_{\mathrm{d}}(\delta_{ik}\delta_{jl} + \delta_{il}\delta_{jk})]\dot{\theta}\sigma_{kl} \,. \tag{7}$$

Comparison with (3) shows that

$$\alpha k/f_{\mathrm{cc}} = \tfrac{1}{3}(2\gamma_{\mathrm{d}} + \gamma_{\mathrm{v}}) \tag{8}$$

and

$$\gamma = (\gamma_{\mathrm{d}} - \gamma_{\mathrm{v}})/(2\gamma_{\mathrm{d}} + \gamma_{\mathrm{v}}) \,. \tag{9}$$

Thelandersson [3] finds the values $\gamma_{\mathrm{v}} = 1.0\alpha/f_{\mathrm{cc}}$ and $\gamma_{\mathrm{d}} = 3.0\alpha/f_{\mathrm{cc}}$ on the basis of two-dimensional experiments. According to (8) and (9) this results in $k = 2.33$ and $\gamma = 0.285$. Note that the result $k = 2.33$ is within the range of values (1.8–2.35) that has been found in uniaxial testing.

3. Constitutive relations for concrete at elevated temperatures

A basic assumption of the smeared crack model as proposed by De Borst, De Borst and Nauta, and Rots et al. [15–18] is the decomposition of the total strain rate $\dot{\boldsymbol{\varepsilon}}$ into a crack strain rate $\dot{\boldsymbol{\varepsilon}}^{\mathrm{cr}}$ and a concrete strain rate $\dot{\boldsymbol{\varepsilon}}^{\mathrm{co}}$:

$$\dot{\boldsymbol{\varepsilon}} = \dot{\boldsymbol{\varepsilon}}^{\mathrm{cr}} + \dot{\boldsymbol{\varepsilon}}^{\mathrm{co}} \,. \tag{10}$$

The crack strain rate $\dot{\boldsymbol{\varepsilon}}^{\mathrm{cr}}$ can again be decomposed into several contributions, thus modelling multiple, non-orthogonal cracking [15, 16]. The actual implementation of this crack model is not the subject of this discussion. Here, we shall focus on deriving the incremental stress–strain relations and tangent operators for cracked under thermal loading conditions.

In the present analysis we assume that the concrete strain rate $\dot{\boldsymbol{\varepsilon}}^{\mathrm{co}}$ is composed of three contributions, namely the elastic strain rate $\dot{\boldsymbol{\varepsilon}}^{\mathrm{e}}$, the thermal strain rate $\dot{\boldsymbol{\varepsilon}}^{\theta}$ and the transient creep strain rate $\dot{\boldsymbol{\varepsilon}}^{\mathrm{tr}}$. When we introduce the matrix $\boldsymbol{C}^{\mathrm{co}}$ which contains the instantaneous elastic compliances, we can set up a bijective relationship between the elastic strain vector $\boldsymbol{\varepsilon}^{\mathrm{e}}$ and the stress vector $\boldsymbol{\sigma}$:

$$\boldsymbol{\varepsilon}^{\mathrm{e}} = \boldsymbol{C}^{\mathrm{co}}\boldsymbol{\sigma} \,. \tag{11}$$

Since the elastic properties have been postulated to be a function of the temperature, we have for the elastic compliance matrix: $\boldsymbol{C}^{\mathrm{co}} = \boldsymbol{C}^{\mathrm{co}}(\theta)$. Accordingly, we obtain for the time derivative

$$\dot{\boldsymbol{\varepsilon}}^{\mathrm{e}} = \boldsymbol{C}^{\mathrm{co}}\dot{\boldsymbol{\sigma}} + \dot{\boldsymbol{C}}^{\mathrm{co}}\boldsymbol{\sigma} \,. \tag{12}$$

Since

$$\dot{\boldsymbol{C}}^{\mathrm{co}} = \frac{\partial \boldsymbol{C}^{\mathrm{co}}}{\partial \theta}\,\dot{\theta} \,, \tag{13}$$

(12) can be written as

$$\dot{\boldsymbol{\varepsilon}}^{\mathrm{e}} = \boldsymbol{C}^{\mathrm{co}}\dot{\boldsymbol{\sigma}} + \dot{\theta}\,\frac{\partial \boldsymbol{C}^{\mathrm{co}}}{\partial \theta}\,\boldsymbol{\sigma}\,. \tag{14}$$

The rate of thermal dilatation $\dot{\boldsymbol{\varepsilon}}^{\theta}$ is given by

$$\dot{\boldsymbol{\varepsilon}}^{\theta} = \alpha\dot{\theta}\boldsymbol{i}\,, \tag{15}$$

while the transient creep rate $\dot{\boldsymbol{\varepsilon}}^{\mathrm{tr}}$ has been defined in (2).

When the elastic strain rate, the thermal strain rate and the transient strain rate are added we obtain for the total strain rate $\dot{\boldsymbol{\varepsilon}}^{\mathrm{co}}$ of the concrete

$$\dot{\boldsymbol{\varepsilon}}^{\mathrm{co}} = \boldsymbol{C}^{\mathrm{co}}\dot{\boldsymbol{\sigma}} + \alpha\dot{\theta}\boldsymbol{i} + \dot{\theta}\,\frac{\partial \boldsymbol{C}^{\mathrm{co}}}{\partial \theta}\,\boldsymbol{\sigma} + \dot{\theta}\boldsymbol{H}\boldsymbol{\sigma}\,. \tag{16}$$

Note that this formulation is accurate only for moderate compressive stresses. If higher stress levels in the compressive domain are to be considered, plastic behaviour of concrete (and temperature influences on the plastic properties) has to be included in the analysis. Incorporation of such models, however, is outside the scope of the present analysis. Another limitation is the fact that hygric influences are also not explicitly taken into account. At moderate temperatures, we observe hygral transport phenomena and an ensuing influence on the strains. Equation (16) is therefore less accurate in such conditions.

Equation (16) has been obtained by simply superimposing elastic deformations, thermal dilatation and the thermomechanical coupling term $\dot{\boldsymbol{\varepsilon}}^{\mathrm{tr}}$. In an alternative strategy Thelandersson [3] proposes to consider the strain rate $\dot{\boldsymbol{\varepsilon}}^{\mathrm{co}}$ as a function not only of the stress $\boldsymbol{\sigma}$ and the temperature θ, but also of their fluxes $\dot{\boldsymbol{\sigma}}$ and $\dot{\theta}$: $\dot{\boldsymbol{\varepsilon}}^{\mathrm{co}} = \dot{\boldsymbol{\varepsilon}}^{\mathrm{co}}(\boldsymbol{\sigma}, \dot{\boldsymbol{\sigma}}, \theta, \dot{\theta})$. Using the representation theorem for isotropic tensor functions and retaining only those terms that are at most linear in the stress tensor $\boldsymbol{\sigma}$ or the stress rate tensor $\dot{\boldsymbol{\sigma}}$, we also arrive at (16).

Before integrating (16) for a finite time step, we briefly recall the equations for the crack formulation [15–18]. We shall restrict the present treatment to a single crack, but the extension to multiple cracking is straightforward [15–17]. We first consider the crack strain rate in a coordinate system that is aligned with the crack axes: $\dot{\boldsymbol{e}}^{\mathrm{cr}} = [\dot{e}^{\mathrm{cr}}_{\mathrm{nn}}, \dot{e}^{\mathrm{cr}}_{\mathrm{nt}}]^{\mathrm{t}}$. $\dot{e}^{\mathrm{cr}}_{\mathrm{nn}}$ is the normal crack strain and $\dot{e}^{\mathrm{cr}}_{\mathrm{nt}}$ is the shear crack strain in this local coordinate system. $\dot{\boldsymbol{e}}^{\mathrm{cr}}$ can be transformed to the global xyz-coordinate system with the aid of 3×2 transformation matrix $\boldsymbol{N}$ [15–18]:

$$\dot{\boldsymbol{\varepsilon}}^{\mathrm{cr}} = \boldsymbol{N}\dot{\boldsymbol{e}}^{\mathrm{cr}}\,. \tag{17}$$

The relation between the stress and the crack strains is most conveniently expressed in the local (crack) coordinate system:

$$\dot{\boldsymbol{e}}^{\mathrm{cr}} = \boldsymbol{C}^{\mathrm{cr}}\dot{\boldsymbol{s}}\,, \tag{18}$$

where $\boldsymbol{C}^{\mathrm{cr}}$ is a 2×2 matrix which contains the compliances of the smeared crack and $\dot{\boldsymbol{s}}$ is the stress rate vector in the crack coordinate system.

Considering the fact that $\dot{\boldsymbol{s}}$ and $\dot{\boldsymbol{e}}^{\mathrm{cr}}$ each contain two components, $\boldsymbol{C}^{\mathrm{cr}}$ is a 2×2 matrix. The off-diagonal terms of this matrix represent the shear–normal coupling, that is the coupling

between normal stresses and shear strains, and between shear stresses and normal strains. These couplings only become significant for large crack strains. For the present purpose they may be assumed to be negligibly small. Accordingly, $\boldsymbol{C}^{\mathrm{cr}}$ reads

$$\boldsymbol{C}^{\mathrm{cr}} = \begin{bmatrix} C_{11}^{\mathrm{cr}} & 0 \\ 0 & C_{22}^{\mathrm{cr}} \end{bmatrix}. \tag{19}$$

Furthermore, the normal and the shear stresses in the crack have been assumed to be linearly related to respectively the normal and the shear crack strain and, in consideration of the aforementioned paucity of experimental data, have been assumed to be independent of the temperature (see also Fig. 1). Consequently, C_{11}^{cr} and C_{22}^{cr} have a constant value. When we have no state changes (e.g. crack formation) during a time step, $\boldsymbol{C}^{\mathrm{cr}}$ and hence $\boldsymbol{C}^{\mathrm{co}} + \boldsymbol{N}\boldsymbol{C}^{\mathrm{cr}}\boldsymbol{N}^{\mathrm{t}}$ are essentially constant matrices, i.e. independent of the stress. It is noted though, that $\boldsymbol{C}^{\mathrm{co}} + \boldsymbol{N}\boldsymbol{C}^{\mathrm{cr}}\boldsymbol{N}^{\mathrm{t}}$ does depend on the temperature since $\boldsymbol{C}^{\mathrm{co}} = \boldsymbol{C}^{\mathrm{co}}(\theta)$.

When $\dot{s}_{\mathrm{nn}}$ is the normal stress rate vector in the crack and $\dot{s}_{\mathrm{nt}}$ is the shear stress rate vector in the crack, we have $\dot{\boldsymbol{s}} = [\dot{s}_{\mathrm{nn}}, \dot{s}_{\mathrm{nt}}]^{\mathrm{t}}$. In a similar fashion as $\dot{\boldsymbol{e}}^{\mathrm{cr}}$ is related to $\dot{\boldsymbol{\varepsilon}}^{\mathrm{cr}}$, the stress rate $\dot{\boldsymbol{s}}$ can be linked to the stress rate in the global coordinate system $\dot{\boldsymbol{\sigma}}$:

$$\dot{\boldsymbol{s}} = \boldsymbol{N}^{\mathrm{t}}\dot{\boldsymbol{\sigma}}\,. \tag{20}$$

Combination of (17), (18) an (20) results in

$$\dot{\boldsymbol{\varepsilon}}^{\mathrm{cr}} = \boldsymbol{N}\boldsymbol{C}^{\mathrm{cr}}\boldsymbol{N}^{\mathrm{t}}\dot{\boldsymbol{\sigma}}\,, \tag{21}$$

so that in consideration of (10) the total strain rate is given by

$$\dot{\boldsymbol{\varepsilon}} = [\boldsymbol{C}^{\mathrm{co}} + \boldsymbol{N}\boldsymbol{C}^{\mathrm{cr}}\boldsymbol{N}^{\mathrm{t}}]\dot{\boldsymbol{\sigma}} + \left[\alpha\boldsymbol{i} + \frac{\partial \boldsymbol{C}^{\mathrm{co}}}{\partial\theta}\,\boldsymbol{\sigma} + \boldsymbol{H}\boldsymbol{\sigma}\right]\dot{\theta}\,. \tag{22}$$

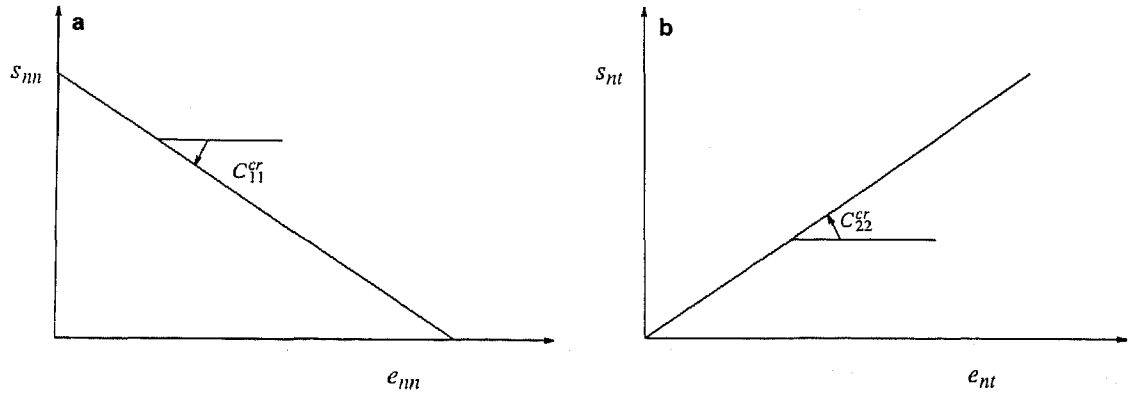

Fig. 1. Dependence of crack stresses on crack strains: (a) normal stress as a function of normal crack strain; (b) shear stress as a function of shear crack strain.

4. Numerical integration and linearisation moduli

For integration of (22) over a finite time step we assume that the stress vector $\boldsymbol{\sigma}$ and the compliance matrix $\boldsymbol{C}^{\mathrm{co}}$ vary linearly in the course of a time step. $\boldsymbol{\sigma}_\tau$ and $\boldsymbol{C}^{\mathrm{co}}_\tau$ refer to the stress vector and the compliance matrix in the beginning of the time step while $\boldsymbol{\sigma}_{\tau+\Delta\tau}$ and $\boldsymbol{C}^{\mathrm{co}}_{\tau+\Delta\tau}$ denote their values at $\tau+\Delta\tau$. At $\tau+\beta\Delta\tau$, $0\leqslant\beta\leqslant 1$, $\boldsymbol{\sigma}$ and $\boldsymbol{C}^{\mathrm{co}}$ are given by

$$\boldsymbol{\sigma}_{\tau+\beta\Delta\tau} = (1-\beta)\boldsymbol{\sigma}_\tau + \beta\boldsymbol{\sigma}_{\tau+\Delta\tau} \tag{23}$$

and

$$\boldsymbol{C}^{\mathrm{co}}_{\tau+\beta\Delta\tau} = (1-\beta)\boldsymbol{C}^{\mathrm{co}}_\tau + \beta\boldsymbol{C}^{\mathrm{co}}_{\tau+\Delta\tau}\,. \tag{24}$$

Rewriting (23) and (24) gives

$$\boldsymbol{\sigma}_{\tau+\beta\Delta\tau} = \boldsymbol{\sigma}_\tau + \beta\Delta\boldsymbol{\sigma} \tag{25}$$

and

$$\boldsymbol{C}^{\mathrm{co}}_{\tau+\beta\Delta\tau} = \boldsymbol{C}^{\mathrm{co}}_\tau + \beta\Delta\boldsymbol{C}^{\mathrm{co}}\,, \tag{26}$$

which, upon substitution in (22), results in

$$\dot{\boldsymbol{\varepsilon}} = [\boldsymbol{C}^{\mathrm{co}}_\tau + \beta\Delta\boldsymbol{C}^{\mathrm{co}} + \boldsymbol{N}\boldsymbol{C}^{\mathrm{cr}}\boldsymbol{N}^{\mathrm{t}}]\dot{\boldsymbol{\sigma}} + \left[\alpha\boldsymbol{i} + \left(\frac{\partial \boldsymbol{C}^{\mathrm{co}}}{\partial\theta} + \boldsymbol{H}\right)(\boldsymbol{\sigma}_\tau + \beta\Delta\boldsymbol{\sigma})\right]\dot{\theta}\,. \tag{27}$$

Note that owing to the fact that the stress–strain relation within the crack has been assumed to be time-independent, $\boldsymbol{C}^{\mathrm{cr}} = \boldsymbol{C}^{\mathrm{cr}}_\tau = \boldsymbol{C}^{\mathrm{cr}}_{\tau+\Delta\tau}$. Integration of (27) and invoking (13) yields

$$\Delta\boldsymbol{\varepsilon} = [\boldsymbol{C}^{\mathrm{co}}_\tau + \beta\Delta\boldsymbol{C}^{\mathrm{co}} + \boldsymbol{N}\boldsymbol{C}^{\mathrm{cr}}\boldsymbol{N}^{\mathrm{t}}]\Delta\boldsymbol{\sigma} + \alpha\Delta\theta\boldsymbol{i} + (\Delta\boldsymbol{C}^{\mathrm{co}} + \Delta\theta\boldsymbol{H})(\boldsymbol{\sigma}_\tau + \beta\Delta\boldsymbol{\sigma})\,. \tag{28}$$

Rearranging (28) we obtain

$$\Delta\boldsymbol{\varepsilon} = [\boldsymbol{C}^{\mathrm{co}}_\tau + \boldsymbol{N}\boldsymbol{C}^{\mathrm{cr}}\boldsymbol{N}^{\mathrm{t}} + \beta(2\Delta\boldsymbol{C}^{\mathrm{co}} + \Delta\theta\boldsymbol{H})]\Delta\boldsymbol{\sigma} + \alpha\Delta\theta\boldsymbol{i} + (\Delta\boldsymbol{C}^{\mathrm{co}} + \Delta\theta\boldsymbol{H})\boldsymbol{\sigma}_\tau\,. \tag{29}$$

When we employ the definitions

$$\boldsymbol{A} = \boldsymbol{C}^{\mathrm{co}}_\tau + \beta(2\Delta\boldsymbol{C}^{\mathrm{co}} + \Delta\theta\boldsymbol{H})\,, \tag{30}$$

$$\Delta\boldsymbol{\varepsilon}^{\mathrm{tr}} = \Delta\theta\boldsymbol{H}\boldsymbol{\sigma}_\tau \tag{31}$$

and

$$\Delta\boldsymbol{\varepsilon}^{\theta} = \alpha\Delta\theta\boldsymbol{i}\,, \tag{32}$$

(29) can be written more simply as

$$\Delta\boldsymbol{\varepsilon} - \Delta\boldsymbol{\varepsilon}^{\theta} - \Delta\boldsymbol{\varepsilon}^{\mathrm{tr}} - \Delta\boldsymbol{C}^{\mathrm{co}}\boldsymbol{\sigma}_\tau = [\boldsymbol{A} + \boldsymbol{N}\boldsymbol{C}^{\mathrm{cr}}\boldsymbol{N}^{\mathrm{t}}]\Delta\boldsymbol{\sigma}\,. \tag{33}$$

We next make use of the Sherman–Morrison–Woodbury formula to obtain the inverse relation

$$\Delta\boldsymbol{\sigma} = [\boldsymbol{\Gamma} - \boldsymbol{\Gamma}\boldsymbol{N}(\boldsymbol{D}^{\mathrm{cr}} + \boldsymbol{N}^{\mathrm{t}}\boldsymbol{\Gamma}\boldsymbol{N})^{-1}\boldsymbol{N}^{\mathrm{t}}\boldsymbol{\Gamma}](\Delta\boldsymbol{\varepsilon} - \Delta\boldsymbol{\varepsilon}^{\theta} - \Delta\boldsymbol{\varepsilon}^{\mathrm{tr}} - \Delta\boldsymbol{C}^{\mathrm{co}}\boldsymbol{\sigma}_{\tau}) , \tag{34}$$

where $\boldsymbol{\Gamma}$ and $\boldsymbol{D}^{\mathrm{cr}}$ have been defined as $\boldsymbol{\Gamma} = \boldsymbol{A}^{-1}$ and $\boldsymbol{D}^{\mathrm{cr}} = [\boldsymbol{C}^{\mathrm{cr}}]^{-1}$. Differentiation of (33) with respect to $\boldsymbol{\sigma}$ gives

$$\frac{\partial\boldsymbol{\varepsilon}}{\partial\boldsymbol{\sigma}} = \boldsymbol{A} + \boldsymbol{N}\boldsymbol{C}^{cr}\boldsymbol{N}^{\mathrm{t}} ,$$

since $\boldsymbol{C}^{\mathrm{cr}}$ has been assumed to be a constant matrix. If $\boldsymbol{C}^{\mathrm{cr}}$ depends on $\boldsymbol{\sigma}$ an additional term arises. Inversion subsequently shows that

$$\boldsymbol{D} = \boldsymbol{\Gamma} - \boldsymbol{\Gamma}\boldsymbol{N}(\boldsymbol{D}^{\mathrm{cr}} + \boldsymbol{N}^{\mathrm{t}}\boldsymbol{\Gamma}\boldsymbol{N})^{-1}\boldsymbol{N}^{\mathrm{t}}\boldsymbol{\Gamma} \tag{35}$$

serves as proper tangent operator if Newton's method is used for the solution of the resulting set of nonlinear algebraic equations on structural level.

It is emphasised that (34) will only predict the stress increment exactly if the stress varies linearly over a time step. This is the assumption on which the algorithm is based (23). If this assumption is violated an error is committed. The magnitude of this error depends on the value of β as will be discussed in a quantitative sense in the next section. If the optimal value of β still gives unacceptable errors the presently used single-step integration rule should be replaced by a higher order scheme (e.g. [21]), but the example calculations do not support the necessity for such a scheme.

The present deviation considers compliance relations, adds all relevant strain rates and then inverts the resulting constitutive relation. As another approach we may set out to derive a stiffness relation directly. The result is given by

$$\Delta\boldsymbol{\sigma} = [\boldsymbol{\Gamma} - \boldsymbol{\Gamma}\boldsymbol{N}(\boldsymbol{D}^{\mathrm{cr}} + \boldsymbol{N}^{\mathrm{t}}\boldsymbol{\Gamma}\boldsymbol{N})^{-1}\boldsymbol{N}^{\mathrm{t}}\boldsymbol{\Gamma}](\Delta\boldsymbol{\varepsilon} - \Delta\boldsymbol{\varepsilon}^{\theta} - \Delta\boldsymbol{\varepsilon}^{\mathrm{tr}} - [\boldsymbol{D}^{\mathrm{co}}_{\tau+\Delta\tau}]^{-1}\Delta\boldsymbol{D}^{\mathrm{co}}\boldsymbol{\varepsilon}^{\mathrm{e}}_{\tau}) , \tag{36}$$

with $\boldsymbol{D}^{\mathrm{co}} = [\boldsymbol{C}^{\mathrm{co}}]^{-1}$ and $\Delta\boldsymbol{D}^{\mathrm{co}} = \boldsymbol{D}^{\mathrm{co}}_{\tau+\Delta\tau} - \boldsymbol{D}^{\mathrm{co}}_{\tau}$. Equation (35) is identical to (34), since it can be shown that

$$[\boldsymbol{D}^{\mathrm{co}}_{\tau+\Delta\tau}]^{-1}\Delta\boldsymbol{D}^{\mathrm{co}}\boldsymbol{\varepsilon}^{\mathrm{e}}_{\tau} = -\Delta\boldsymbol{C}^{\mathrm{co}}\boldsymbol{\sigma}_{\tau} . \tag{37}$$

It has been assumed that the matrix $\boldsymbol{H}$ which governs the distribution of the transient creep strains has an isotropic structure. If the elastic behaviour of the concrete is governed by an isotropic elastic law throughout the entire heating process (which is a reasonable assumption to moderate stress levels), $\boldsymbol{\Gamma}$ can be calculated explicitly. Calculation of $\boldsymbol{\Gamma}$ is then tantamount to modifying Young's modulus E and Poisson's ratio ν into $\bar{E}$ and $\bar{\nu}$, respectively. To show this we first write

$$A_{ijkl} = -\frac{\bar{\nu}}{\bar{E}}\,\delta_{ij}\delta_{kl} + \frac{1+\bar{\nu}}{2\bar{E}}\,[\delta_{ik}\delta_{jl} + \delta_{il}\delta_{jk}] \tag{38}$$

and

$$[C^{\mathrm{co}}_{ijkl}]_{\tau} = -\frac{\nu_{\tau}}{E_{\tau}}\,\delta_{ij}\delta_{kl} + \frac{1+\nu_{\tau}}{2E_{\tau}}\,[\delta_{ik}\delta_{jl} + \delta_{il}\delta_{jk}] , \tag{39}$$

and we recall that $\Delta \boldsymbol{C}^{co} = \boldsymbol{C}^{co}_{\tau+\Delta\tau} - \boldsymbol{C}^{co}_{\tau}$. From (30), (38) and (39) we can now derive that

$$\frac{1+\bar{\nu}}{\bar{E}} = (1-2\beta)\frac{1+\nu_\tau}{E_\tau} + 2\beta\frac{1+\nu_{\tau+\Delta\tau}}{E_{\tau+\Delta\tau}} + \beta\Delta\theta\frac{(1+\gamma)\alpha k}{f_{cc}} \tag{40}$$

and

$$-\frac{\bar{\nu}}{\bar{E}} = -(1-2\beta)\frac{\nu_\tau}{E_\tau} - 2\beta\frac{\nu_{\tau+\Delta\tau}}{E_{\tau+\Delta\tau}} - \beta\Delta\theta\frac{\gamma\alpha k}{f_{cc}}\,, \tag{41}$$

which can be solved to give

$$\bar{E} = \frac{E_\tau}{1-2\beta\Delta E/E_{\tau+\Delta\tau} + \beta\Delta\theta E_\tau \alpha k/f_{cc}} \tag{42}$$

and

$$\bar{\nu} = \frac{\nu_\tau - 2\beta(\nu_\tau - \nu_{\tau+\Delta\tau}E_\tau/E_{\tau+\Delta\tau}) + \beta\Delta\theta\gamma E_\tau \alpha k/f_{cc}}{1-2\beta\Delta E/E_{\tau+\Delta\tau} + \beta\Delta\theta E_\tau \alpha k/f_{cc}} \tag{43}$$

with $\Delta E = E_{\tau+\Delta\tau} - E_\tau$.

It is interesting to scrutinise the classical case that $k = 0$ somewhat closer. In that case (42) and (43) reduce to

$$\bar{E} = \frac{E_\tau}{1-2\beta\Delta E/E_{\tau+\Delta\tau}} \tag{44}$$

and

$$\bar{\nu} = \frac{\nu_\tau - 2\beta(\nu_\tau - \nu_{\tau+\Delta\tau})E_\tau/E_{\tau+\Delta\tau}}{1-2\beta\Delta E/E_{\tau+\Delta\tau}}\,. \tag{45}$$

When creep effects are not taken into account, we have the total (secant) stress–strain relation at $\tau + \Delta\tau$

$$\boldsymbol{\varepsilon}_{\tau+\Delta\tau} = \boldsymbol{C}^{co}_{\tau+\Delta\tau}\boldsymbol{\sigma}_{\tau+\Delta\tau}\,, \tag{46}$$

which can be brought in an exact incremental form

$$\Delta\boldsymbol{\varepsilon} = \boldsymbol{C}^{co}_{\tau+\Delta\tau}\Delta\boldsymbol{\sigma} + \Delta\boldsymbol{C}^{co}\boldsymbol{\sigma}_\tau\,, \tag{47}$$

so that in an exact incremental approach $E_{\tau+\Delta\tau}$ and $\nu_{\tau+\Delta\tau}$ serve as the pseudo-elastic moduli. We observe that the choice $\beta = \frac{1}{2}$ also yields $\bar{E} = E_{\tau+\Delta\tau}$ and $\bar{\nu} = \nu_{\tau+\Delta\tau}$, which shows that in the absence of creep strains a midpoint integration rule ($\beta = \frac{1}{2}$) is exact.

5. Examples

In this section we will consider some examples. First we will scrutinise the properties of the solution algorithm outlined in the preceding section. Next we will simulate the behaviour of plain concrete cylinders under thermal loading conditions. The section will be concluded with an analysis of a reinforced one-way slab subjected to a fire test.

Assessment of the solution algorithm

Before predictions are made with a numerical program it must be checked carefully for its consistency and proper implementation. This is best done by numerical simulation of a problem that is also tractable with analytical tools. For this purpose we shall consider an initially unstressed plane stress element which is constrained at the bottom and at the top and is heated from 0 to 200°C. To make an analytical solution possible the material properties have been assigned constant values; $\alpha = 12 \cdot 10^{-6}\,°C^{-1}$, $E = 30000\ N/mm^2$ and $f_{cc} = 40\ N/mm^2$. The material parameter k for the transient creep has been assigned the value 2.35.

Because of the lack of strain rate components which are caused by cracking or degradation of the elastic properties, the total strain rate consists of an elastic component, a component due to thermal dilatation and a contribution caused by transient creep. The boundary conditions require that the total strain rate be zero, so that

$$\dot{\boldsymbol{\varepsilon}}^{e} + \dot{\boldsymbol{\varepsilon}}^{\theta} + \dot{\boldsymbol{\varepsilon}}^{tr} = 0\,.$$

The individual contributions are given by $\dot{\boldsymbol{\varepsilon}}^{e} = \dot{\boldsymbol{\sigma}}/E$, $\dot{\boldsymbol{\varepsilon}}^{\theta} = \alpha\dot{\theta}$ and $\dot{\boldsymbol{\varepsilon}}^{tr} = k\alpha\dot{\theta}\boldsymbol{\sigma}/f_{cc}$, which results in the following differential equation:

$$\frac{\dot{\sigma}}{E} + \alpha\dot{\theta} + \frac{k\alpha}{f_{cc}}\,\dot{\theta}\sigma = 0\,.$$

This differential equation can be solved to give

$$\sigma = -\frac{f_{cc}}{k}\,(1 - \exp\,(-Ek\alpha\theta/f_{cc}))\,.$$

The analytical result has been plotted in Fig. 2. In order to assess the influence of β three calculations have been carried out, namely for $\beta = 0$, $\beta = \frac{1}{2}$ and $\beta = 1$. The results are represented in Fig. 2 for the case that temperature steps are taken of 40°C. The calculation with the mid-point rule $\beta = \frac{1}{2}$ matches the analytical solution most closely, but all solutions approach the analytical solution if the time step is made smaller.

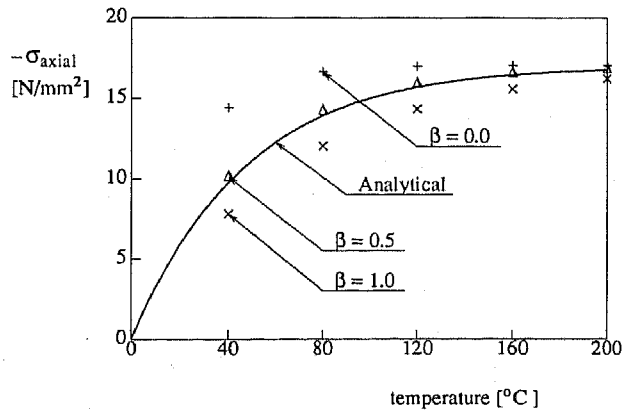

Fig. 2. Axial stress as a function of the temperature. Analytical and numerical results.

Further, the impact of using a proper tangent operator has been assessed. To this end calculations have been carried out for temperature steps of 40°C, 66.7°C and 100°C. A mid-point integration rule has been used for all the calculations. It appeared that if an elastic stiffness matrix is used instead of a proper tangent the calculation becomes unstable for temperature steps of 100°C.

Simulation of tests on plain concrete cylinders

Anderberg and Thelandersson [1] have conducted experiments on plain concrete cylinders in order to investigate the mechanical behaviour at high temperatures. Two series of experiments have been carried out. In the first series of experiments the temperature increase was 1°C/min while the second series was exposed to a temperature increase of 5°C/min. No significant differences were observed between both test series and an approximately homogeneous temperature distribution was observed in the specimens.

Since we now set out to simulate the true material behaviour the assumption of constant material properties which has been made in the preceding example no longer suffices. Instead Young's modulus E, the linear coefficient of thermal dilatation α and the compressive strength f_{cc} are now assumed to be a function of the temperature. The experimentally determined relationships and the adopted idealisation are shown in Fig. 3, in which the value of each material parameter has been plotted relative to its value at room temperature. For both experiments to be discussed the initial value of Young's modulus was $E = 21500\,\mathrm{N/mm^2}$ and the initial value of the coefficient of thermal dilatation was $\alpha = 12 \cdot 10^{-6}\,^{\circ}\mathrm{C}^{-1}$. In the first experiment $f_{cc} = 34.7\,\mathrm{N/mm^2}$ while for the second specimen it was equal to $f_{cc} = 41.3\,\mathrm{N/mm^2}$. In the analyses that take into account transient behaviour, a value of 2.35 has been adopted for k.

The first experiment that has been simulated is a concrete cylinder that is fully restrained in the vertical direction. The results of the numerical simulations with and without the effect of transient creep strains as well as the experimental data have been plotted in Fig. 4. In the beginning of the experiment the cylinder is stress-free. Because of the increasing temperature the structure will dilate which is prevented by the boundary conditions. This causes a compressive stress in the specimen. For the analysis that includes the effect of transient creep strains the compressive stress reaches a maximum around 200°C. For higher temperatures the decreasing Young's modulus causes an overall decrease in the stress until the specimen has become stress-free at 800°C, i.e., when the Young's modulus has been reduced to zero.

The agreement between the experiment and the model simulation is quite reasonable, at least in a qualitative sense. Quantitatively, there are some deviations between simulation and experiment, in particular in the beginning of the test and between 100°C and 200°C. The deviation at the onset of loading may be due to misalignment of the loading plates and the concrete cylinder. The deviation in the temperature traject between 100°C and 200°C can be explained by the neglect of moisture transport phenomena. As argued before these influences are particularly important in this temperature regime. The analysis which does not consider transient creep strains shows an overly stiff response compared with the experimental measurements. When $\theta = 171\,^{\circ}\mathrm{C}$ the axial stress becomes equal to the compressive strength, thus causing failure of the specimen.

The second experiment that has been simulated is a cylinder which has been loaded

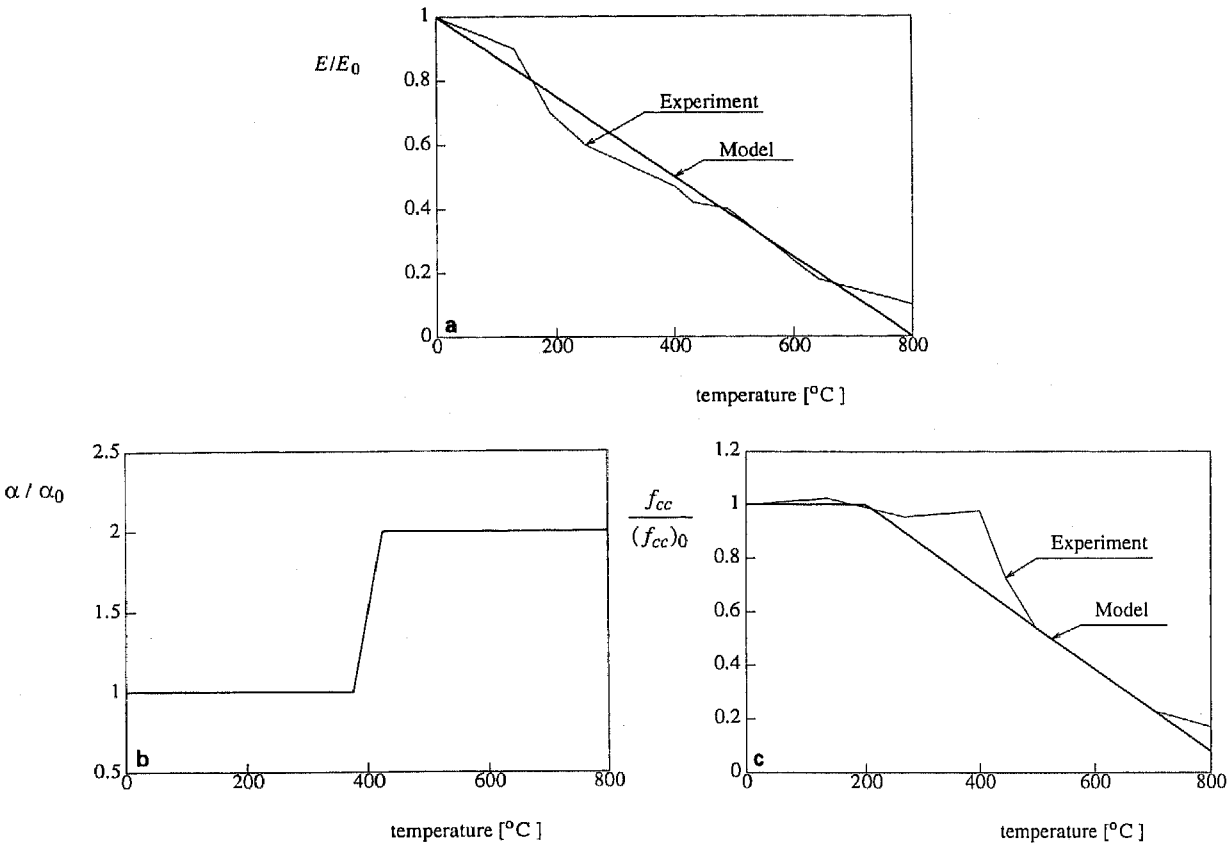

Fig. 3. Material parameters of concrete as a function of the temperature: (a) Young's modulus; (b) linear coefficient of thermal dilatation; (c) compressive strength.

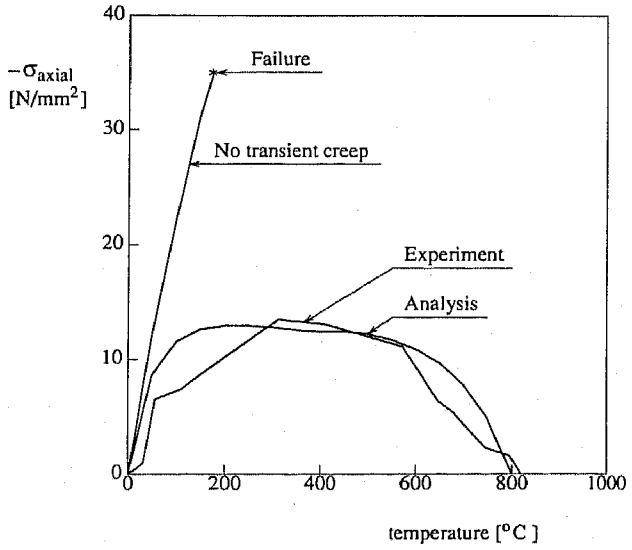

Fig. 4. Axial stress as a function of the temperature for the restrained concrete cylinder.

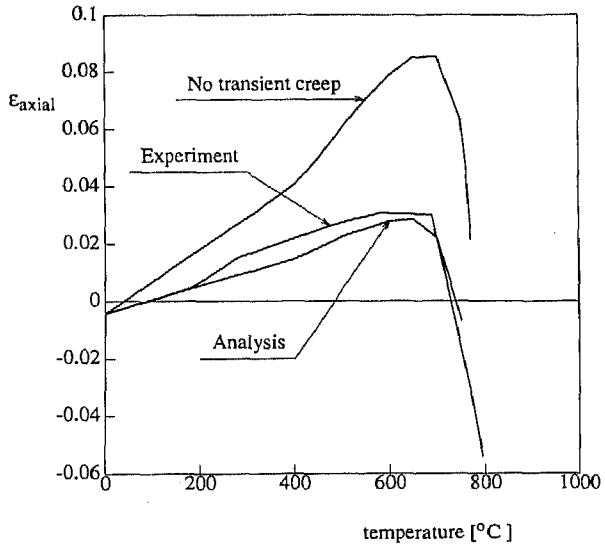

Fig. 5. Axial strain as a function of the temperature for the unrestrained concrete cylinder.

uniaxially to 22.5% of its compressive strength at room temperature. The strain that has been measured as well as model simulations with and without the effect of transient creep strains have been plotted in Fig. 5 as a function of the temperature. Around 750°C the uniaxial compressive strength has been reduced to such an extent that failure occurs. Again, the agreement between experiment and the numerical simulation that includes the effect of transient creep strains is good, especially if we consider the relatively coarse multilinear idealisation of the development of the material properties with temperature. The analysis without transient creep strains shows far too much volumetric expansion compared with the experimental measurements.

Simulation of a fire test on a reinforced concrete slab

In the next example the influence of cracking on the structural behaviour has also been taken into account. The example concerns two reinforced concrete one-way slabs which have been subjected to a fire test at the University of Gent [10]. The slabs were simply supported on the short sides while the displacements at the other two sides were free. The slabs were first loaded by two jacks over the full width, whereafter their bottom was heated uniformly. Because of these boundary and loading conditions the slabs could be analysed as beams. The finite element idealisation of both slabs, which will be denoted as G1 and G3 in conformity with the experiment, is shown in Fig. 6. Eight-noded plane stress elements with four-point

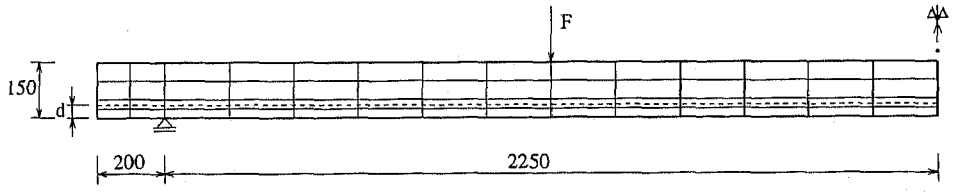

Fig. 6. Finite element idealisation for reinforced concrete slabs tested at the University of Gent [10].

Table 1
Geometry and loading data for reinforced concrete slabs

	Slab G1	Slab G3
Width (mm)	1900	1900
d (mm)	15	35
Reinforcement (mm^2)	1178	1414
Self-weight q (kN/m)	6.29	6.89
Line load F (kN/m)	14.5	14.6

Table 2
Material properties of concrete at room temperature

	Slab G1	Slab G3
E (N/mm^2)	45200	39800
ν	0.2	0.2
α(°C^{-1})	0.000012	0.000012
f_c(N/mm^2)	42.7	43.0
f_t(N/mm^2)	2.6	2.6
C_{11}^{cr}(mm^2/N)	−0.000902	−0.000902
C_{22}^{cr}(mm^2/N)	0.000212	0.000241

Gauss integration have been used in both analyses. The geometrical data and the loading intensity are listed in Table 1 for both slabs.

The values of the concrete properties at room temperature are listed in Table 2. Because the dependence of the material parameters on the temperature is not given in [10], the dependence of the compressive strength and the coefficient of thermal expansion on the temperature have been assumed to be identical to the relations that have been plotted in Fig. 3, while Young's modulus has been assigned a slightly different dependence on the temperature (Fig. 7). In consideration of the lack of experimental data regarding a possible dependence of Poisson's ratio on the temperature, this material parameter has been assigned a constant value: $\nu = 0.2$. The transient creep coefficients k and γ have been assigned the following values: $k = 2.35$ and $\gamma = 0.2$. Especially the estimation of the latter parameter is rather crude. The choice is based on Thelandersson's [3] multiaxial data, which suggest that γ has approximately the same value as Poisson's ratio ν. Note that the assumptions that ν has a constant value for the entire temperature regime and that $\gamma = \nu$, lead to an extremely simple form of (42) and (43). There is also a paucity of experimental data with regard to the dependence of tensile strength on the temperature [20]. For this reason the constant value $f_{ct} = 2.6\,\mathrm{N/mm^2}$ has been used. Furthermore a linear descending branch has been used to model the tension-stiffening effect with an ultimate uniaxial strain $\varepsilon_u = f_{sy}/E_s$. f_{sy} and E_s are respectively the yield strength and Young's modulus of the reinforcing steel at room temperature.

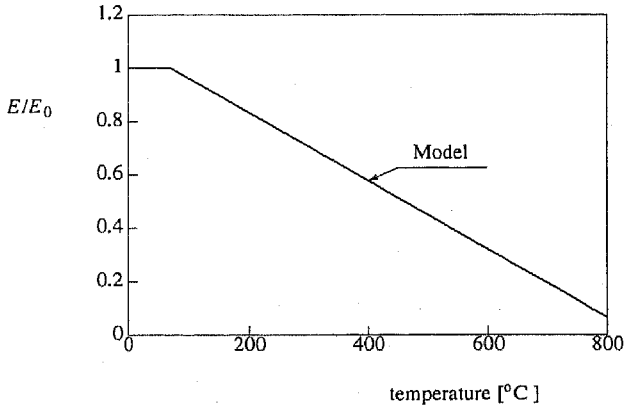

Fig. 7. Dependence of Young's modulus on the temperature as used in the analysis of reinforced concrete slabs.

As alluded to in the preceding the material properties of the reinforcement are a function of the temperature [9]. In particular the yield strength f_{sy} and Young's modulus E_s depend on the temperature. The specific relationships that have been adopted in the present simulations are shown in Fig. 8. The values at room temperature are listed in Table 3.

An accurate estimate of the temperature distribution through the thickness of the slab is very important for correctly determining the strains and stresses in the slab in the course of the heating process. From experimental data [10] the temperature distributions as shown in Fig. 9 have been extracted for the various time steps. It has been assumed that this distribution through the thickness is the same everywhere in the slab, although this is doubtlessly a rather course idealisation of reality.

The finite element simulations of both slabs yielded time-deflection curves as represented in Fig. 10. We observe that slab G3 exhibits a much more ductile behaviour than slab G1. This is because the concrete cover of slab G3 is thicker. Consequently, the temperature increase of the reinforcement takes place at a later stage and also the degradation of the stiffness of the reinforcement is postponed. The overall agreement with the experimental data is quite

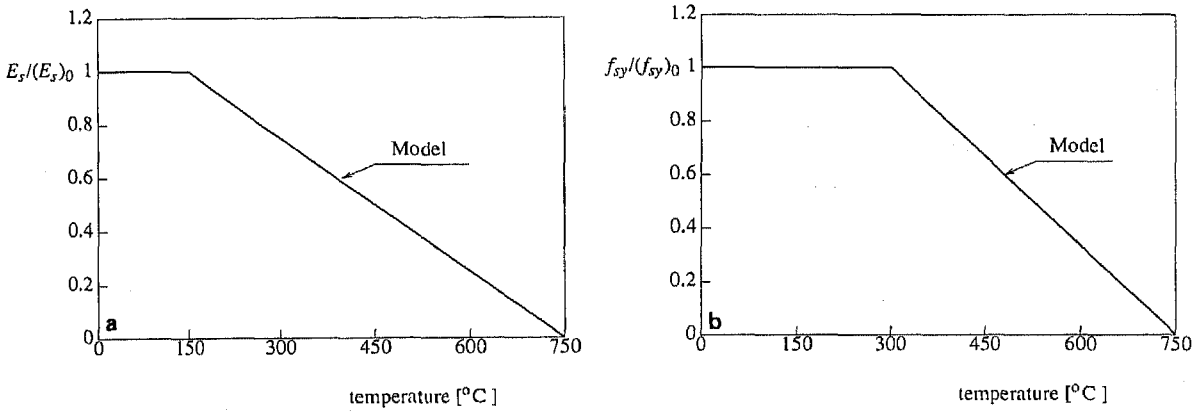

Fig. 8. Material parameters of steel as a function of the temperature: (a) Young's modulus; (b) yield strength.

Table 3
Material properties of reinforcement at room temperature

	Slab G1	Slab G3
E_s (N/mm^2)	215000	215000
f_{sy} (N/mm^2)	504	504

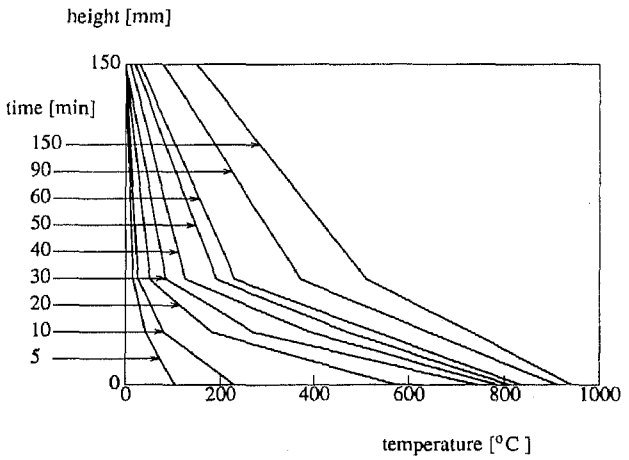

Fig. 9. Temperature distribution through the thickness of the slab for different times.

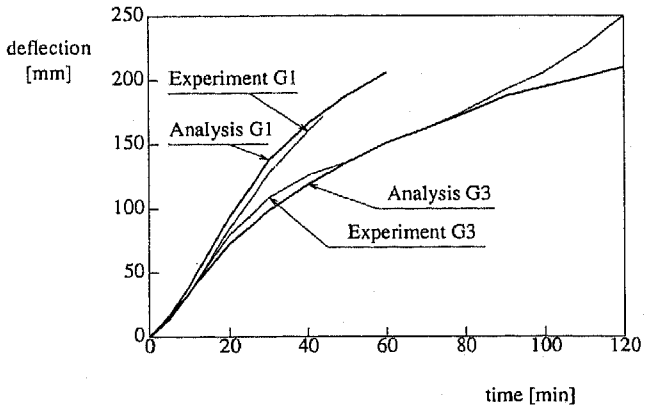

Fig. 10. Measured and calculated time-deflection curves for reinforced concrete slabs.

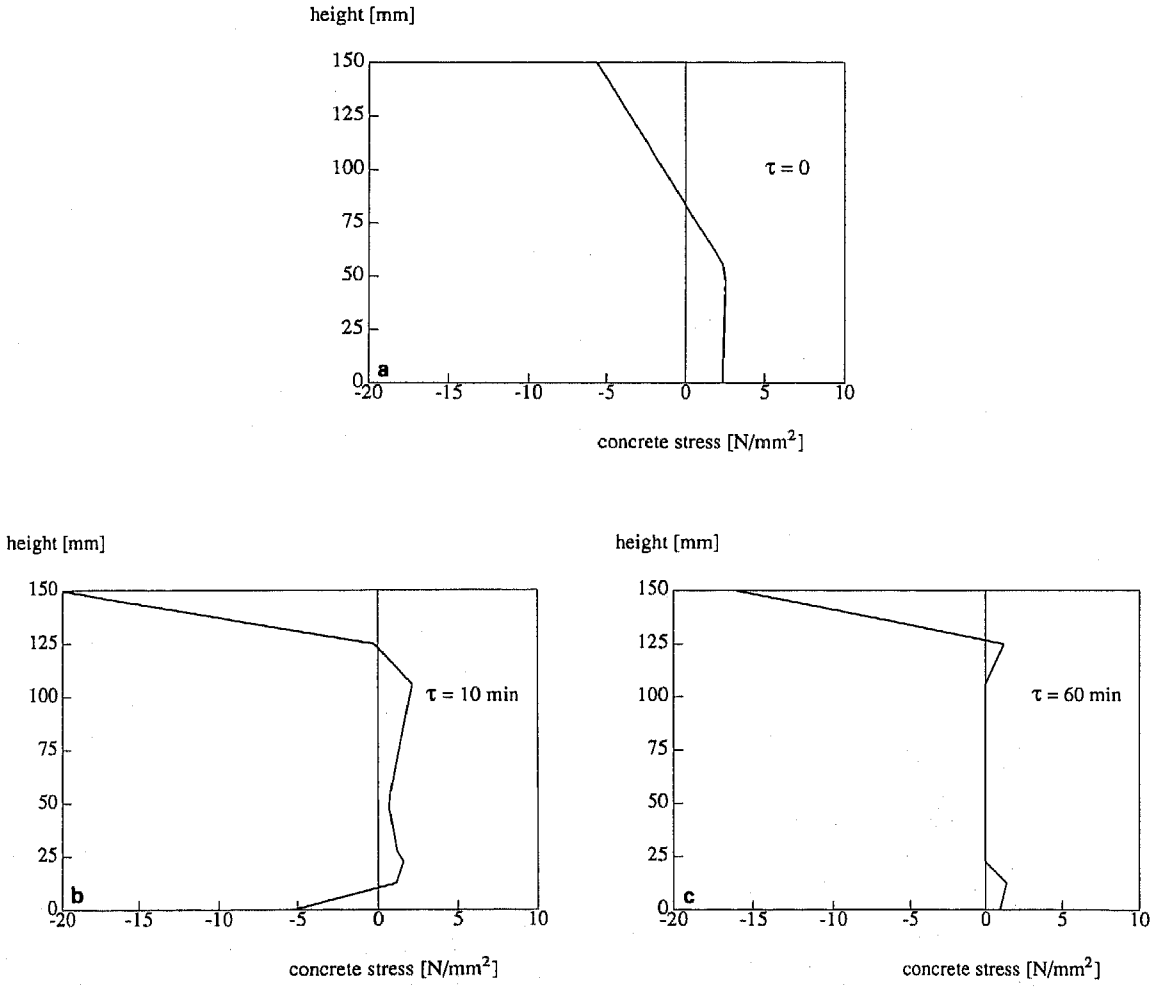

Fig. 11. Profiles of horizontal normal stress over the height of the slab G1: (a) $\tau = 0$; (b) $\tau = 10$ min; (c) $\tau = 60$ min.

reasonable. It is noted that in the experiment the measurements have been terminated when the deflection of the centre of the slab exceeded 150 mm for slab G1, while the measurements of slab G3 have been continued until structural failure.

More interesting than the time-deflection curves are the horizontal normal stresses in the centre of the slab. In Fig. 11 these stresses have been plotted through the thickness of slab G1 for three different stages in the heating process. At $\tau = 0$, so at the onset of the fire test, we observe that the top of the slab is loaded in compression, while the bottom of the slab is cracked. The reinforcement is loaded in tension. At $\tau = 10$ min we observe the impact of the nonlinear temperature distribution through the thickness. The lowermost fibres are now loaded in compression owing to the effect of thermal dilatation. At $\tau = 60$ min the middle of the cross-section is completely cracked. The deflections are so big, that the lower fibres again have to sustain tensile stresses. On further heating the reinforcing steel will reach the yield strength and failure will occur.

6. Conclusions

In this paper models and algorithms have been discussed for the analysis of concrete structures, reinforced or not, which are subjected to thermal loadings. The discussed theory and the presented simulations support the following statements.

Incorporation of the phenomenon of transient creep is indispensable for obtaining accurate simulations of concrete structures which are exposed to extreme temperature conditions. Any analysis of a concrete structure subject to thermal loading which ignores this phenomenon may be grossly in error. A three-dimensional model has been developed, calibrated with experimental data [3] and implemented in the three-dimensional finite element code.

Classical smeared crack formulations cannot be extended to deal with concrete structures that are exposed to thermal loading, at least not when modern fracture mechanics-based crack propagation theories are employed. This observation is similar to the fact that classical smeared crack formulations cannot be used in the prediction of long-term behaviour of concrete members [15, 16]. A proper solution to this problem involves a rigorous resolution of the total strain rate into a concrete and a crack strain rate.

In this paper a consistent algorithm has been developed which simultaneously considers the effects of thermal dilatation, degradation of the elastic properties with increasing temperature, transient creep and smeared cracking. Explicit as well as implicit versions of the algorithm have been considered. The implicit mid-point rule appeared to perform superior.

No attention has been paid to the issue of possible loss of parabolicity of the governing field equations owing to the fact that a strain-softening law has been used for cracking of concrete and that the Young's modulus has been made in a descending function of the temperature. A closer examination of this issue should definitely be undertaken in the future.

Acknowledgment

The calculations have been carried out with the DIANA finite element code of the TNO Institute for Building Materials and Structures. The contributions of the second author were part of his graduation project under supervision of Professor J. Blaauwendraad.

References

[1] Y. Anderberg and S. Thelandersson, Stress and deformation characteristics of concrete at high temperatures: 2. Experimental investigation and material behaviour model, Bulletin 54, Lund Institute of Technology, Lund, 1976.
[2] Y. Anderberg and S. Thelandersson, A constitutive law for concrete at transient high temperature conditions, ACI Specialty Publication SP-55-8, Detroit (1978) 187–205.
[3] S. Thelandersson, Modelling of combined thermal and mechanical action in concrete, ASCE J. Engrg. Mech. 113 (1987) 893–906.
[4] G.A. Khoury, B.N. Grainger and P.J.E. Sullivan, Transient thermal strain of concrete: literature review, conditions within specimen and behaviour of individual constituents, Magazine of Concrete Research 37 (1985) 131–144.
[5] G.A. Khoury, B.N. Grainger and P.J.E. Sullivan, Strain of concrete during first heating to 600°C under load, Magazine of Concrete Research 37 (1985) 195–215.
[6] H.W. Reinhardt, Mechanical and physical properties of concrete between −109°C and +400°C (in Dutch), Cement 31 (1979) 7–13.
[7] U. Schneider, Behaviour of concrete at high temperatures. Deutscher Auschuss für Stahlbeton, Heft 337 (Ernst & Sohn, Berlin, 1982).
[8] U. Schneider, U. Diederichs and C. Ehm, Effect of temperature on steel and concrete for PCRV's, Nucl. Engrg. Design 67 (1981) 245–258.
[9] Y. Anderberg, Behaviour of steel at high temperatures, RILEM State-of-the-Art Report 44-PHT, (RILEM, Paris, 1983).
[10] R. Minne and M. Vandamme, Resistance of reinforced concrete floor slabs against fire (in Dutch), Cement 34 (1982) 642–646.
[11] R.J. van Foeken, Numerical analyses of reinforced concrete structures at high temperatures including cracking, plasticity and creep, in: R.W. Lewis and K. Morgan, eds., Numerical Methods in Thermal Problems, Vol. 4 (Pineridge, Swansea, 1985) 1127–1138.
[12] D.R.J. Owen, J.A. Figueiras and F. Damjanić, Finite element analysis of reinforced and prestressed concrete structures including thermal loading, Comput. Methods Appl. Mech. Engrg. 41 (1983) 323–366.
[13] Y.R. Rashid, Analysis of prestressed concrete pressure vessels, Nucl. Engrg. Design 7 (1968) 334–344.
[14] M. Suidan and W.C. Schnobrich, Finite element analysis of reinforced concrete, ASCE J. Struct. Div. 99 (1973) 2109–2122.
[15] R. de Borst, Smeared cracking, plasticity, creep and thermal loading—A unified approach, Comput. Methods Appl. Mech. Engrg. 62 (1987) 89–110.
[16] R. de Borst, Computational aspects of smeared crack analysis, in: E. Hinton and D.R.J. Owen, eds., Computational Modelling of Reinforced Concrete Structures, Chapter 2 (Pineridge, Swansea, 1986) 44–83.
[17] R. de Borst and P. Nauta, Non-orthogonal cracks in a smeared finite element model, Engrg. Computations 2 (1985) 35–46.
[18] J.G. Rots, P. Nauta, G.M.A. Kusters and J. Blaauwendraad, Smeared crack approach and fracture localization in concrete, Heron 30 (1) (1985) 1–48.
[19] R.W. Litton, A contribution to the analysis of concrete structures under cyclic loading, Ph.D. Thesis, University of California, Berkeley, California, 1974.
[20] W. Brameshuber and H.K. Hilsdorf, Development of strength and deformability of very young concrete, in: S.P. Shah, S.E. Schwartz, eds., Preprints SEM-RILEM Internat. Conf. on Fracture of Concrete and Rock, Houston, TX (1987) 655–667.
[21] J.H. Argyris, L.E. Vaz and K.J. Willam, Improved solution methods for inelastic rate problems, Comput. Methods Appl. Mech. Engrg. 16 (1978) 231–277.